Eur. Phys. J. D **29**, 7–16 (2004)
DOI: 10.1140/epjd/e2004-00016-4

THE EUROPEAN PHYSICAL JOURNAL D

Theoretical study of the Lyman γ line profile of atomic hydrogen perturbed by collisions with protons

Lyman γ line profile

N.F. Allard[1,2,a], J.F. Kielkopf[3,b], G. Hébrard[1], and J.M. Peek[4]

[1] Institut d'Astrophysique de Paris, CNRS, 98bis boulevard Arago, 75014 Paris, France
[2] Observatoire de Paris-Meudon, LERMA, 92195 Meudon Principal Cedex, France
[3] Department of Physics, University of Louisville, Louisville, KY 40292, USA
[4] 45 Puye, Los Alamos, NM 87544, USA

Received 1st July 2003
Published online 17 February 2004 –

Abstract. The far wings of the Lyman series of atomic hydrogen exhibit satellites, enhancements that may be associated with quasi-molecular states of H_2 and H_2^+. Quasi-molecular satellites in the red wings of Lyman α and Lyman β were previously identified in the spectra of the DA white dwarfs. We present here new theoretical calculations of Lyman γ profiles perturbed by protons. They allow a large feature near 995 Å in UV spectra of hot white dwarfs to be identified. This feature is a blend of two quasi-molecular Lyman γ satellites due to $H-H^+$ collisions near 992 Å and 996 Å.

PACS. 32.70.Jz Line shapes, widths, and shifts

1 Introduction

This paper is a continuation of previous work devoted to radiative collision effects in the Lyman series of atomic hydrogen used to interpret the spectra of hydrogen-rich white dwarf stars and laboratory plasmas.

The line wing, generally, does not decrease monotonically with increasing frequency separation from the line center. Its shape, for an atom in the presence of other atoms, ions, or electrons, is sensitive to the difference between the initial and final state interaction potentials. When this difference, for a given transition, goes through an extremum, a relatively wider range of interatomic distances contribute to the same spectral frequency, resulting in an enhancement, or *satellite*, in the line wing. Satellites in alkali spectra have been known since the 1930's [1]. More recently, satellites associated with the molecular interactions of H_2 and H_2^+ have been discovered in stars and in laboratory plasmas in the far wings of Lyman series lines [2–4].

The stars which show Lyman α satellites are cool DA white dwarfs, old *Horizontal Branch* stars of spectral type A, and the λ Boötis stars [5–7]. Satellites on the Lyman β line of atomic hydrogen due to collisions of the neutral atom with protons were observed in spectra of hot DA white dwarfs [3,8–10]. Features near 995 Å suspected to be new satellites in the wing of Lyman γ provided motivation for the present work in which we investigate the theory of the Lyman γ line profile.

The theoretical potentials for the binary interactions of one hydrogen atom with another hydrogen atom or ion now may be computed with high accuracy. This allows us to solve the radiative collision problem given an appropriate theoretical framework for the lineshape. Structures in stellar spectra observed in the Lyman α and Lyman β line wings have been very well described by a theoretical model atmosphere which uses the line profile theory and calculations of Allard et al. [11–14]. Here we will evaluate the unified line shape theory [14], briefly reviewed in Section 2, including the complex manifold of excited diatomic states states asymptotically leading to the $n = 4$ state of the hydrogen atom.

For this purpose, since published calculations do not include all of the states that are needed, a new consistent set of accurate theoretical H_2^+ molecular potentials was computed, and used to describe the interaction between radiator and protons for the line shape. The results of the potential calculation are summarized in Section 2.2.

In this work we are still limited by a lack of knowledge of the dependence of the radiative transition dipole moment on atom-ion separation for highly excited states. For the purpose of this evaluation we suppose it to be constant and equal to its asymptotic value. Although the shape of the line satellites should depend on the R-dependent electric-dipole moment and we suspect the remaining

[a] e-mail: allard@iap.fr
[b] e-mail: kielkopf@louisville.edu

discrepancies between the observed spectra and our calculations are due to this assumption of constant dipole moment, we think this is a good first approximation especially for the interactions at large R which dominate the line profile under the conditions of interest. The Lyman γ profiles and satellites are calculated for low densities appropriate for the application to white dwarfs and for higher densities for application to laboratory experiments at temperatures likely to be encountered in those sources. These results are presented in Section 3. We used them to predict synthetic spectra for hot DA white dwarfs and to confirm our identification of the Lyman γ satellites in observed spectra as described in Section 4.

2 Theoretical line profiles

2.1 General expression of the spectrum

A detailed description of our unified theory of the shape of the Lyman lines has been given by Allard et al. [11,14]. Here we will only review it briefly, and then describe how we treat the problem of the large number of excited atomic states that must be included to calculate the Lyman series beyond the first few members.

The spectral line is given as the Fourier transform of a correlation function

$$F_\nu(\Delta\nu) = \mathbf{FT}\left[\exp\left(ng(s)\right)\right]. \tag{1}$$

The Fourier transform is taken such that $F_\nu(\Delta\nu)$ is normalized to unity when integrated over all frequencies, and $\Delta\nu$ is measured relative to the unperturbed line.

The autocorrelation function is calculated with the following assumptions: (1) the radiator is stationary in space; (2) the perturbers are mutually independent; (3) in the adiabatic approach valid in the present case the interaction potentials give contributions which are scalarly additive.

For a transition $\alpha = (i, f)$ from initial state i to final state f, we have

$$\begin{aligned} g_\alpha(s) = & \frac{1}{\sum_{e,e'}{}^{(\alpha)} |d_{ee'}|^2} \\ & \times \sum_{e,e'}{}^{(\alpha)} \int_0^{+\infty} 2\pi\rho d\rho \int_{-\infty}^{+\infty} dx\ \tilde{d}_{ee'}[R(0)] \\ & \times \left[e^{\frac{i}{\hbar}\int_0^s dt\ V_{e'e}[R(t)]}\ \tilde{d}^*{}_{ee'}[R(s)] - \tilde{d}_{ee'}[R(0)]\right]. \end{aligned} \tag{2}$$

The e and e' label the energy surfaces on which the interacting atoms approach the initial and final atomic states of the transition as $R \to \infty$ (R denotes the internuclear distance between the radiator and the perturber). The asymptotic initial and final state energies are E_i^∞ and E_f^∞, such that $E_e(R) \to E_i^\infty$ as $R \to \infty$. We then have R-dependent frequencies

$$\nu_{e'e}(R) \equiv (E'_e(R) - E_e(R))/h \tag{3}$$

which become the isolated radiator frequency ν_{if} when perturbers are far from the radiator. The total line strength of the transition is $\sum_{e,e'} |d_{ee'}|^2$. At time t from the point of closest approach for a rectilinear classical path we have:

$$R(t) = \left[\rho^2 + (x + vt)^2\right]^{1/2}, \tag{4}$$

where ρ is the impact parameter of the perturber trajectory, v is the relative velocity, and x is the position of the perturber along its trajectory. We define $\tilde{d}_{ee'}(R(t))$ as a *modulated* dipole

$$\tilde{d}_{ee'}[R(t)] = d_{ee'}[R(t)] e^{-\frac{\beta}{2}V_e[R(t)]}. \tag{5}$$

The difference potential is

$$\Delta V(R) = V_{e'e}(R) = V_{e'}(R) - V_e(R), \tag{6}$$

where the potential energy for the state is

$$V_e(R) = E_e(R) - E_e^\infty. \tag{7}$$

In the above, we neglect the influence of the potentials $V_e(R)$ and $V_{e'}(R)$ on the perturber trajectories, which remain straight lines. Although we should drop the Boltzmann factor $e^{-\beta V_e(R)}$ for consistency with our straight trajectory approximation, by keeping it we improve the result in the wings where its effects are significant.

The dipole moment of the quasi-molecular transition is supposed to be slowly varying with the interatomic distance and consequently can be considered as constant and equal to its asymptotic value for this first calculation of the spectrum. However, to keep track of the excited states and establish which ones contribute, an H_2^+ correlation diagram is constructed for Lyman γ. It is an extension to higher states of the work explained in a previous paper [11]. Table 1 gives us the states of the united atom correlated to the $n = 1$ and $n = 4$ levels of the separated atoms.

2.2 Diatomic potentials

At moderate pressures the spectral line intensity profile is related to perturbations of the radiating atom in isolated binary collision events. The gas is imagined to consist of pairs of nearest atoms in states of collision, or equivalently, of diatomic molecules in free states of nuclear motion. The adiabatic interaction of the radiating neutral hydrogen atom with a proton is described by potential energies $V_e(R)$ for each electronic state of H_2^+. Tables of accurate theoretical potentials leading asymptotically to the $n = 1, 2, 3$ atomic states have been published [15], and were suitable for computing profiles of Lyman α and β, but many more states are needed for Lyman γ. Also, with increased excitation of the atom, the interactions extend to larger interatomic distances and the line shape calculations require potentials at larger R and a finer sampling than usually tabulated. For these reasons we computed the exact solutions for the states of H_2^+ that were of interest.

Table 1. Correlation diagram of H_2^+ for Lyman γ.

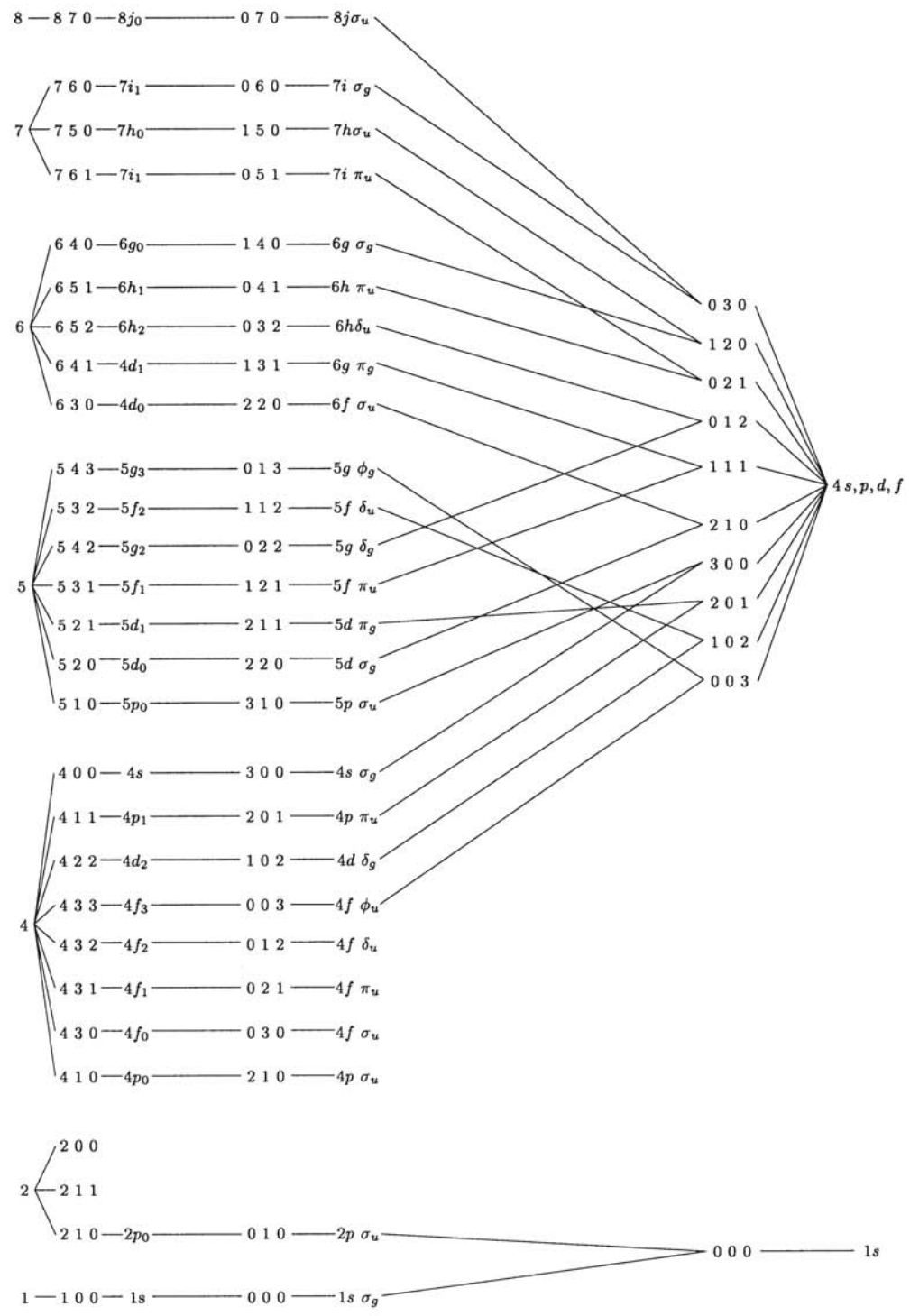

H_2^+ is a special case of two homopolar positive charges at a fixed distance R interacting with an electron, a one-electron diatomic molecule (OEDM). Neglecting nuclear motion, the Schrödinger equation for a general OEDM about centers a and b is separable in elliptic coordinates $\xi = (r_a + r_b)/R$, $\eta = (r_a - r_b)/R$ and, ϕ, the azimuthal angle [16,17]. The wavefunctions may be specified by the number of nodes in each coordinate, the nodal quantum numbers n_ξ, n_η, and $n_\phi = m$.

Simple analytic expressions for the solutions cannot be found, but exact numerical solutions can be computed. Although systematic tabulations of the lower states of H_2^+ exist [15], the work of Power [16,17] provides a framework for fast exact calculations. To describe these solutions we follow, roughly, the discussion of Bates and Reid [18].

The quantum numbers for this system become those of a hydrogenic atom as R approaches its limiting values at $(0, \infty)$.

The azimuthal quantum number, m, is a good quantum number but differs from the atomic case. The energy is degenerate and independent of the sign of m but does depend on its absolute value. In the following, $|m|$ indicates the absolute value. The value of $|m|$ is independent of R. That is, it is a good quantum number for this system. Values of $(|m| = 0, 1, 2, 3, ...)$ correspond to the molecular orbital symbols $(\sigma, \pi, \delta, \phi, ...)$.

The principle quantum number is preserved only in the $(0, \infty)$ limits for R and is designated by (n_u, n_s) in those limits where u refers to the united atom and s to the separated atoms.

The orbital angular momentum quantum number is also preserved only in the $(0, \infty)$ limits of R and is designated (ℓ_u, ℓ_s) in these limits. The value for ℓ_u does determine the gerade/ungerade symmetry of the molecule (inversion through a midpoint in R) which is designated by the g, u subscripts on the Greek symbol associated with $|m|$. The state is gerade for even values of ℓ_u and ungerade for odd ℓ_u values.

The common designation of the molecular orbital consists of the set of symbols labeling n_u, ℓ_u, $|m|$, and (g, u). An example would be $2p\sigma_u$ where $n_u = 2$, $\ell_u = 1$, and $m = 0$. Clearly, the use of ℓ_u and the (g, u) subscript is redundant. The number ℓ_u has been replaced by the usual letter appropriate to the atom case. Another designation would be to use n_s and ℓ_s instead of n_u and ℓ_u.

The nodal quantum numbers are related to the atomic quantum numbers by

$$n_\xi = n_u - \ell_u - 1 \tag{8}$$

$$n_\eta = \ell_u - |m| \tag{9}$$

$$n_\phi = |m| \tag{10}$$

for the united atom limit [16]. As R goes to infinity, the elliptic coordinates become parabolic coordinates and the asymptotic solutions provide a starting point for the exact OEDM solution. The quantum numbers for these solutions are usually given as n_1, n_2, and m, where n_1 is taken to be the same as n_ξ. The separated atom principle quantum number is

$$n_s = n_1 + n_2 + |m| + 1 \tag{11}$$

so the nodal numbers become

$$n_\xi = n_s - n_2 - |m| - 1 \tag{12}$$

$$n_\eta = 2n_2 \text{ (gerade) or } 2n_2 + 1 \text{ (ungerade)} \tag{13}$$

and

$$n_\phi = |m| \tag{14}$$

for the separated atom limit of a homonuclear molecule such as H_2^+ [11,16].

One rule that can be used to construct a correlation diagram is that the number of nodes in the electronic wave function does not change as R changes. The resulting correlation diagram is termed diabatic, rather than adiabatic, which has different rules. The connection between the limiting quantum numbers using this property can be established [18] as

$$n_s = n_u - \frac{1}{2}(\ell_u - |m|) \tag{15}$$

for $(\ell_u - m)$ even and

$$n_s = n_u - \frac{1}{2}(\ell_u - |m| + 1) \tag{16}$$

if $(\ell_u - |m| + 1)$ is even. Table 1 illustrates the correlation diagram in detail for the $n_s = 1$ and $n_s = 4$ states needed for Lyman γ. The diagram for $n_s = 2$ is given in reference [11].

The calculations which we use here were based on Power's OEDM eigenvalue code [19] with modifications by J. Peek to permit double precision calculation with the current generation of Fortran compilers. (The Intel Fortran Compiler (IFC) for Linux, was used in this instance.) We computed all of the low-lying states with $n_s \leq 4$ on a mesh in R as small as 0.25 atomic units out to 120 atomic units. This is well beyond the R at which asymptotic formulas are valid, 96 atomic units in the case of $7h\sigma_0$, for example. While the calculations are exact, Power [16] notes that to ensure convergence to the desired root, the initial guess must be closer to this root than to any other root with the same quantum number m and same symmetry. We have used small increments in R and double precision to help avoid this pitfall. The H $(n = 4)$ state generates the ten pairs of molecular potentials indicated in Table 1. The results for this state are shown graphically in Figure 1. For other lower states (not shown) the agreement for the potential energy with the Madsen and Peek published tabulations [15] was good to all 13 decimal places in atomic units. Since these computations are independent, it leads us to have confidence in the resulting potential curves.

The dipole selection rules for the states in the transition are simple to state:

1. the change in $|m|$ must be either zero or unity;
2. the change in ℓ_u must be odd. Alternatively, the transition must be between gerade and ungerade states;
3. there are no restrictions on the change in n_u.

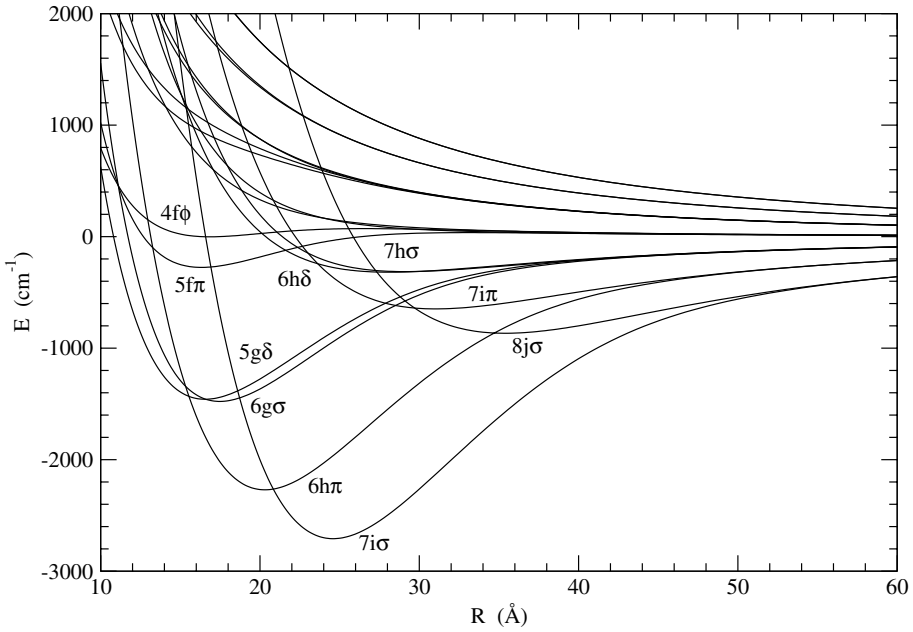

Fig. 1. Molecular potentials for H_2^+ dissociating to the $n = 4$ state of H. The energies are given relative to the asymptotic atomic state. States with potential wells are labeled.

We are aware of no systematic discussions of the structure of the dipole matrix elements. The large-R limiting value for the dipole matrix elements is not known for this system. Even so, the large-R value may not be an accurate estimate at the internuclear separation at which satellites occur. It is known that zeros for $0 < R < \infty$ exist for some dipole transitions in homonuclear OEDM [20–22], including those that contribute to Lyman γ. The importance of these zeros for the line profile is not yet understood.

2.3 Prediction of satellite lines in Lyman γ wing

By applying the selection rules noted above, we see that only transitions between states of opposite parity and having $\Delta|m| = 0, 1$ are dipole allowed. Using this we can deduce which molecular transitions contribute to Lyman γ. Table 2 lists the transitions and their weight given by equation (26) of reference [11].

In radiative collision transitions it is the difference potential between the final and initial states that determines the frequency and the energy emitted or absorbed by a single photon. The spectrum depends additionally on the transition probability for such events. Several transitions are of particular interest and are listed in Table 3. For each one the difference potential exhibits one minimum which, in principle, leads to a corresponding satellite feature in the wing of Lyman γ.

Line satellite positions, intensities, and shapes are functions of three characteristic parameters of the interatomic potentials involved in the transition. Two of these parameters are reported in Table 3.

The first one is the value $\Delta\nu_{H_2^+}$ of the extrema of the potential difference $\Delta V(R)$. The unified theory [1,23] predicts that there will be satellites centered periodically at frequencies corresponding to the extrema of the difference

Table 2. Transitions contributing to Lyman γ.

upper level	lower level	atomic transition	weight
$5p\,\sigma_u$	$1s\,\sigma_g$	(300) − (000)	1
$4s\,\sigma_g$	$2p\,\sigma_u$	(300) − (000)	1
$5d\,\sigma_g$	$2p\,\sigma_u$	(210) − (000)	1
$6f\,\sigma_u$	$1s\,\sigma_g$	(210) − (000)	1
$6g\,\sigma_g$	$2p\,\sigma_u$	(120) − (000)	1
$7h\,\sigma_u$	$1s\,\sigma_g$	(120) − (000)	1
$7i\,\sigma_g$	$2p\,\sigma_u$	(030) − (000)	1
$8j\,\sigma_u$	$1s\,\sigma_g$	(030) − (000)	1
$5d\,\pi_g$	$2p\,\sigma_u$	(201) − (000)	2
$4p\,\pi_u$	$1s\,\sigma_g$	(201) − (000)	2
$6g\,\pi_g$	$2p\,\sigma_u$	(111) − (000)	2
$5f\,\pi_u$	$1s\,\sigma_g$	(111) − (000)	2
$7i\,\pi_g$	$2p\,\sigma_u$	(021) − (000)	2
$6h\,\pi_u$	$1s\,\sigma_g$	(021) − (000)	2

(n_1, n_2, m) correspond to the number of nodes in the wave functions.

potential between the upper and lower states,

$$\Delta\nu_k \ \left(\mathrm{cm}^{-1}\right) = k\Delta\nu_{H_2^+},\ (k = 1, 2, ...) \qquad (17)$$

$\Delta\nu_k$ is the frequency difference between the center of the unperturbed spectral line and the satellite feature, measured for convenience in the same units as the potential energy difference. This series of satellites is due to many-body interactions, and the kth satellite corresponds to the simultaneous presence of k perturbers in the collision volume. Such multi-perturber satellites have been observed in alkali spectra [1,24].

The second one is R_m, the internuclear separation at which the difference potential is an extremum, the line

Table 3. Satellites of Lyman γ due to $H-H^+$ collisions.

upper level	lower level	label	$\Delta\nu_{H_2^+}$ (cm^{-1})	$\lambda_{H_2^+}$(Å)	R_m(Å)
$7i\,\sigma_g$	$2p\,\sigma_u$	1	–2754	1002	25
			–2530	996.5[b]	
			–2505	996.5[c]	
$6h\,\pi_u$	$1s\,\sigma_g$	2	–2284	995	20.6
			–2070	992[b]	
			–2080	992[c]	
$6g\,\sigma_g$	$2p\,\sigma_u$	3	–1470	989	18
			–1280	984.2[b]	
			–1300	983.5[c]	
$8j\,\sigma_u$	$1s\,\sigma_g$	4	–904	984	36
			–750	980[b]	
			–780	980[c]	
$7i\,\pi_g$	$2p\,\sigma_u$	5	–671	981	31.6
			–530	978[b]	
			–540	978[b]	
$7h\,\sigma_u$	$1s\,\sigma_g$	6	–305	978	29.6
			–216	974[b]	
$5f\,\pi_u$	$1s\,\sigma_g$	7	–260	977	16.6
			–200	974[b]	

[a] Predicted, [b] individual profile, [c] total profile.

satellite being predominantly due to perturbers at this distance. The average number of perturbers in the interaction volume at R_m is the determining parameter for the amplitude of the satellites on the spectral line [1,25,26]. It will increase as R_m^2, creating intense satellites from long range extrema.

The third one is the curvature of the difference potential at R_m. A large curvature results in a broad diffuse satellite, but a low curvature leads to a much sharper feature. In Figure 2 we have plotted the H_2^+ difference potentials $\Delta V(R)$ that exhibit a shallow minimum at a large internuclear separation. The relatively long range of the well should produce strong satellites. The low curvature in these wells leads to spectra that are not as broad compared to features appearing in Lyman α.

3 Study of Lyman profiles perturbed by protons

The line profiles have been computed at a temperature of 25 000 K, for different densities of protons from 10^{16} to 10^{18} cm^{-3}.

3.1 Quasi-molecular satellites of Lyman γ

The total profile of Lyman γ depends on many individual transitions, each contribution given by the Fourier transform of an autocorrelation function for one component.

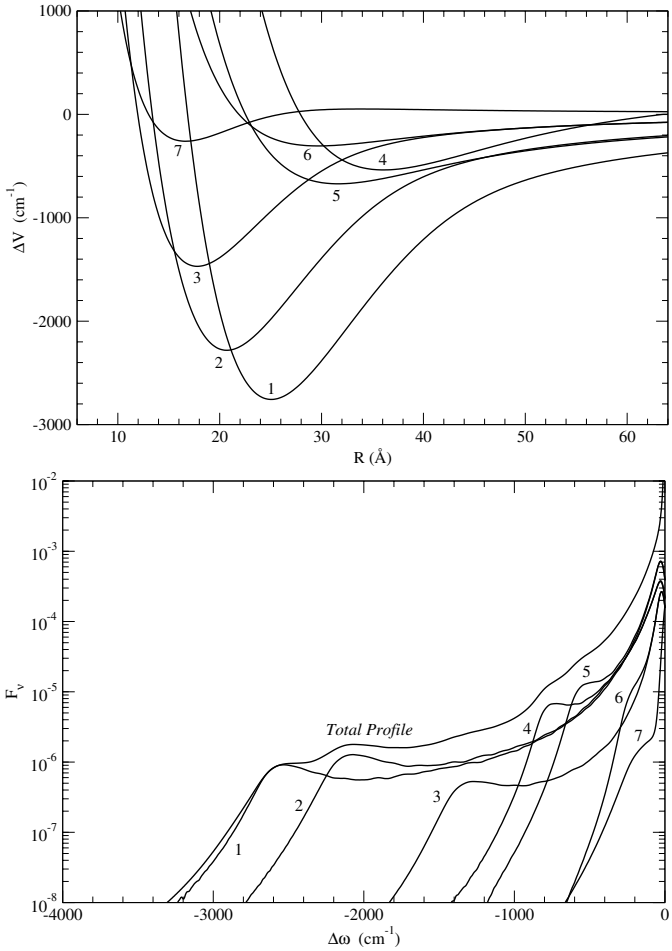

Fig. 2. For Lyman γ, above, potential energy differences which have a minimum; below, corresponding profiles for the individual components compared to the total one. See Table 3 for transition identifications.

Figure 2 shows these profiles separately. The wavelengths of the line satellites are assigned to their transitions in Table 3.

Five distinct satellites or blends of satellites are obvious in the total profile. There are shoulders on the line core at 984 Å, 980 Å, and 978 Å. The two satellites forming in a flat depression of the potential at 31.6 Å and 36 Å produce exceptionally strong satellites: this large atom-ion separation enhances multiple-perturber effects when the density increases, which is responsible for a red asymmetry of the near wing of the total profile. There are prominent features at 992 and 996 Å which blend in the total profile giving a shape similar to the 995 Å feature observed in WD spectra (Fig. 3).

The profile dependence on ion density is shown in Figure 4. The general shape is changing very fast between 10^{17} and 10^{18} cm^{-3} and a general calculation rather than an expansion in density has to be done to get accurate profiles. Consequently these computed profiles are valid from the center to the far wing and allow a comparison of the amplitudes of the satellites to the line core. The line shape consists of a line core in which the intensity

Table 4. Satellites in the Lyman series due to H–H^+ collisions.

Lyman	upper level	lower level	$\Delta\nu_{H_2^+}$ (cm^{-1}) predicted	λ (Å) predicted	λ (Å) observed[a]	R (Å)
α	$4f\ \sigma_u$	$1s\ \sigma_g$	–1240	1234	1230	11.0
	$3d\ \sigma_g$	$2p\ \sigma_u$	–11080	1405	1400	4.5
β	$6h\ \sigma_u$	$1s\ \sigma_g$	−1185	1037	1037	20
	$5g\ \sigma_g$	$2p\ \sigma_u$	−5045	1081	1080	13
	$4f\ \pi_u$	$1s\ \sigma_g$	−3507	1063	1060	10
γ	$8j\ \sigma_u$	$1s\ \sigma_g$	–904	984	984	36
	$7i\ \sigma_g$	$2p\ \sigma_u$	–2754	1002	996	25
	$6h\ \pi_u$	$1s\ \sigma_g$	–2284	995	992	20.6

[a] White dwarf spectra.

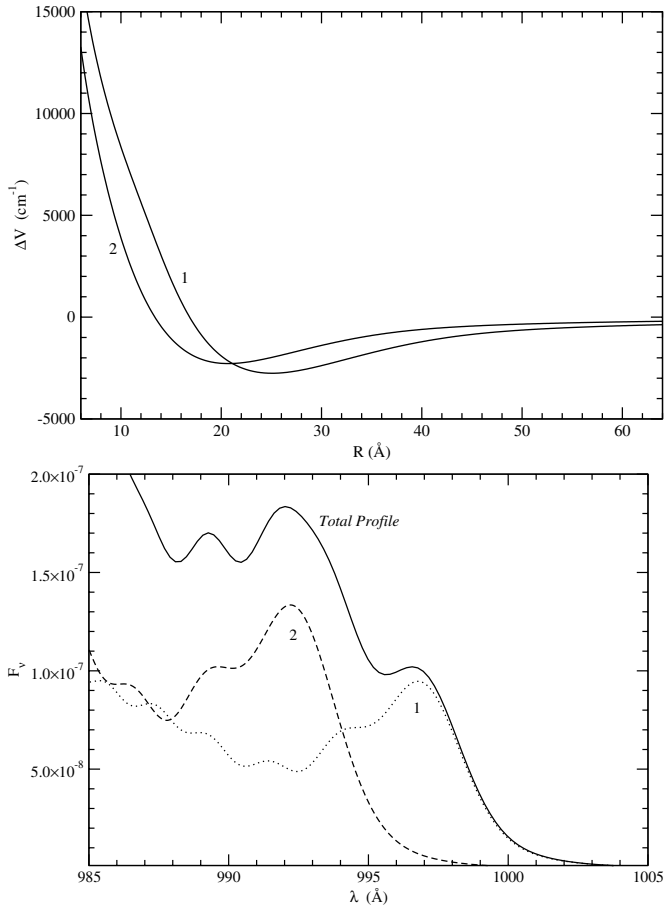

Fig. 3. Above, potential differences of the transitions responsible for Lyman γ satellites close to 995 Å; below, corresponding profiles for the individual components compared to the total one. See Table 3 for transition identifications.

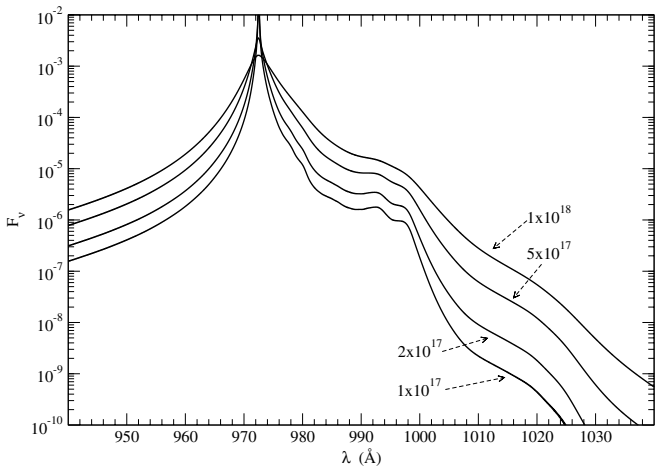

Fig. 4. Variation of the Lyman γ profile with ion density, shown for 1×10^{17}, 2×10^{17}, 5×10^{17}, and 1×10^{18} cm^{-3}.

decreases with increasing proton density and a near wing with the line satellites. In the range of low densities appropriate to white dwarf or λ Boötis stars the satellite amplitude increases linearly with the average number of perturbers because there is a higher probability of binary collisions than many-body collisions. The expansion of the autocorrelation function in powers of density as described in references [11,27] is used only at the lowest density ($\leq 10^{17}$ cm^{-3}).

3.2 Observed satellites in Lyman lines due to H–H^+ collisions

Table 4 lists the wavelengths of the main satellites due to H−H^+ collisions with the upper and lower state identifications and the distance of the atom-ion pair at which the potential extremum occurs. Several of these features are observed in spectra of stars.

The satellites of the higher states are formed by shallow potential extrema at larger interatomic separations, and consequently are close to the main line and rapidly become stronger compared to the main line as the ion density increases.

The one-perturber approximation neglects the contribution of the core of the line, and is valid only in the wing, and in the limit of densities low enough that multiple perturber effects there may be neglected. In practice it is not useful in the Lyman series when the the ion density is larger than 10^{17} cm^{-3}. Figure 5 shows the Lyman γ satellites for densities above 3×10^{17} cm^{-3}, and Figure 6 shows Lyman β satellites for comparison.

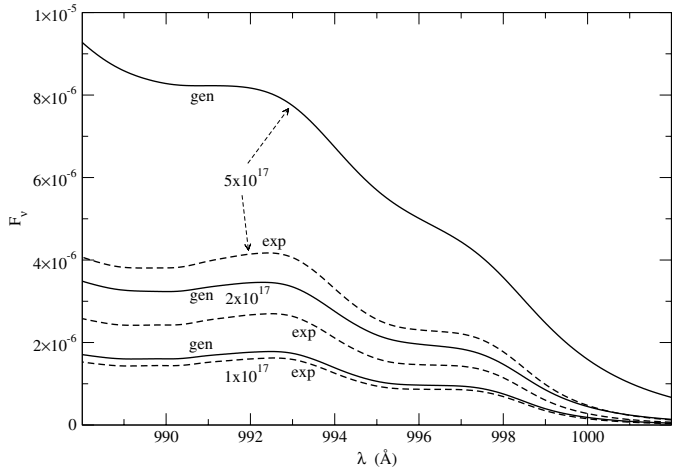

Fig. 5. Comparison of the Lyman γ satellites obtained with expansion of the autocorrelation function in powers of density and with general calculations.

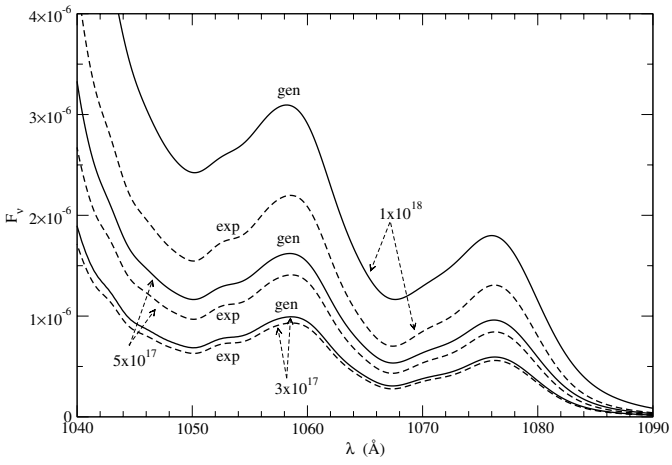

Fig. 6. Comparison of the Lyman β satellites obtained with expansion of the autocorrelation function in powers of density and with general calculations.

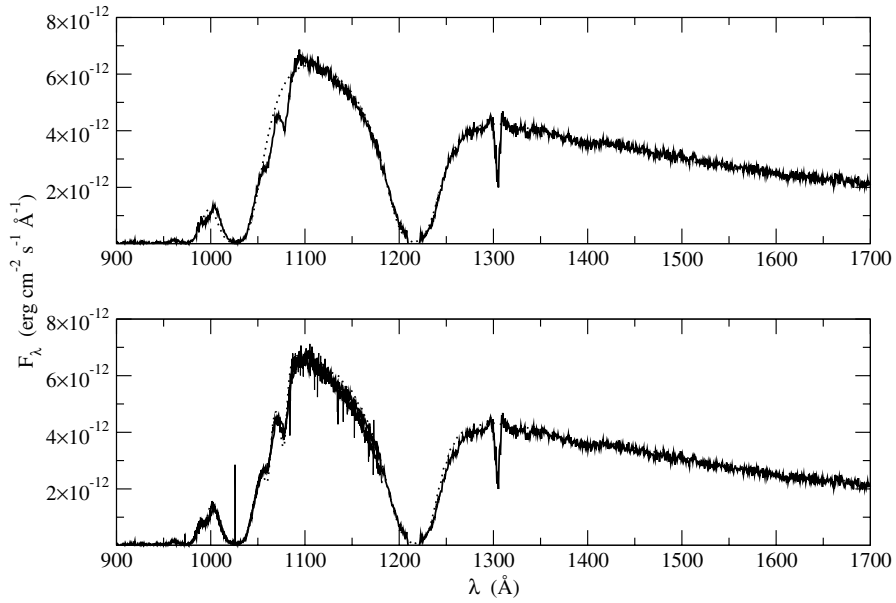

Fig. 7. Upper panel: *HUT* spectrum of the white dwarf Wolf 1346 (—) compared with a synthetic spectrum calculated with the standard VCS Stark broadening theory (···). Lower panel: *FUSE* spectrum (below 1180 Å) and *HUT* spectrum (above 1180 Å) compared to a synthetic spectrum including quasi-molecular satellites. Synthetic spectra are calculated for $\log g = 8$ and $T_{\mathit{eff}} = 20\,000$ K.

For each line the satellites that appear as shoulders near the unperturbed line center are due to shallow minima at large internuclear distances. The distinct satellites farther from the line center form in the deeper potential wells that occur at closer atom-ion separation. The most intense feature seen in laboratory experiments is at 1234 Å, as shown in Figure 3 of Kielkopf and Allard [28]. The satellite is intense because it occurs at an atom-ion separation $R \approx 11$ Å, the interaction volume is therefore large, and the probability that a collision will contribute to this part of the line is high. In the spectra of cool white dwarf stars this satellite due to $H-H^+$ collisions is lost in the Lyman α wing due to H−H. There are two very distinct satellites observed both in stellar and laboratory spectra, one due to ions at 1400 Å, and the other due to neutrals at 1600 Å [2,5–7,28]. The 1400 Å satellite is visible in the Hopkins Ultraviolet Telescope (*HUT*) spectra of the white dwarf star Wolf 1346, but it is at the limit of its visibility as shown in Figure 7. So far, the Lyman β satellites have been observed only in white dwarf spectra, although laboratory experiments are in progress. They appear very distinctly in the *HUT* spectrum, and also in a spectrum of Wolf 1346 taken with the Far Ultraviolet Spectroscopic Explorer (*FUSE*) satellite as shown in Figure 7. The two close Lyman γ satellites blend to make a broad absorption depression in the near red wing in the example shown in Figure 8. Two satellites predicted at 1037 Å and 984 Å for the near red wings of Lyman β and Lyman γ also appear in Figure 8.

4 Comparison of observations with theoretical spectra of DA white dwarfs

We considered an LTE model atmosphere with pure hydrogen composition that explicitly include the Lyman α

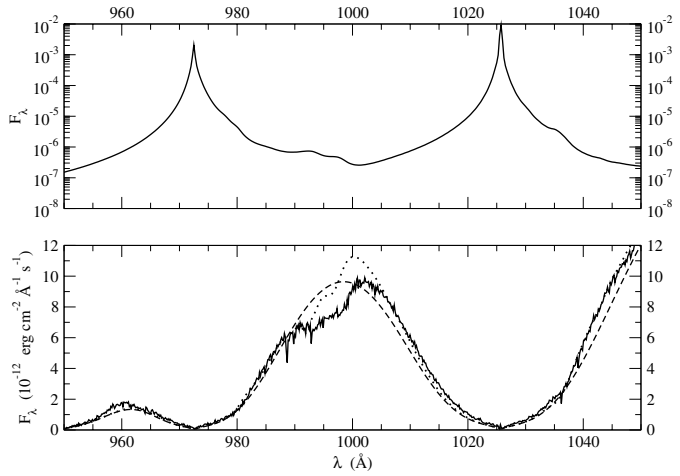

Fig. 8. Above, Lyman γ profile perturbed by H−H$^+$. The density of protons is 2×10^{17} cm^{-3}, and the temperature 25 000 K. Below, *FUSE* spectrum of CD-38° 10980 compared with a theoretical synthetic spectrum for $\log g = 7.9$ and $T_{\mathit{eff}} = 23\,000$ K, and with VCS theory (- - - -).

and Lyman β quasi-molecular opacities in order to make a more detailed comparison of the theoretical spectra with these and other observations.

The Lyman α and Lyman β profiles were computed including perturbations by proton collisions using the H_2^+ potentials of Madsen and Peek [15] and transition dipole moments of Ramaker and Peek [20], and also including neutral atom perturbations using the potentials and dipole moments of Spielfiedel [29]. Atmosphere models and resulting spectra were calculated with programs TLUSTY and SYNSPEC [30–32]. Synthetic spectra were computed in this way to include quasi-molecular satellites of Lyman α, Lyman β, and Lyman γ. The resulting models predict that the Lyman γ satellites are visible for effective temperatures roughly between 15 000 K and 30 000 K.

Observations of the DA white dwarf Wolf 1346 with *HUT* revealed a line shape very different from the expected simple Stark broadening with satellite features appearing near 1078 and 1060 Å as shown in the upper panel of Figure 7. These features were identified as Lyman β satellites due to quasi-molecular H_2^+ [3].

The feature near 995 Å in the red wing of Lyman γ was observed in the *HUT* spectrum shown in Figure 7 and subsequently in spectra recorded by the Orbiting Retrievable Far and Extreme Ultraviolet Spectrograph *ORFEUS* [8]. It was suspected then to be a Lyman γ satellite. We show here that indeed this is the correct explanation. The lower panel of Figure 7 compares our calculations with the *HUT* and *FUSE* observations of this white dwarf. This Lyman γ wing feature is also clearly visible in the spectrum of the white dwarf CD −38°10980 shown in Figure 8. This star's temperature is near the upper limit for the expected visibility range of the Lyman β satellites in white dwarfs. The agreement indicates that the large feature near 995 Å is due to the blend of two close Lyman γ satellites at 991 and 996 Å.

5 Discussion and conclusion

The good agreement between the observed spectra and our calculations allowed the identification of line satellites near 995 Å in white dwarf spectra. The fit, however, is not perfect. The discrepancy appears mainly in a small systematic shift between the predicted and observed spectra shown in Figure 8 [33].

We have investigated the possibility that the simple treatment of perturber velocity used in the profile calculations might be a reason for the discrepancy. Three sets of calculations were made to explore the sensitivity of the profile to different methods of handling the velocity. The first and simplest one used a single mean velocity

$$\bar{v} = (8kT/\pi\mu)^{1/2}, \tag{18}$$

where μ is the reduced mass of the atoms. The second one includes the effects of the distribution of velocities of the perturbers by taking an integral over the Maxwell-Boltzmann distribution of energies with 12 Gauss-Laguerre points. The effect of the distribution would be to pick up contributions from the slowly moving ions, which should sharpen the profile near the singular satellite region, and possibly shift the peak of the satellite. A third run explicitly included the Boltzmann factor $\exp(-\beta V_e(R))$ for the profile in absorption to allow for the initial state probability. The effect of the Boltzmann factor should improve the result in the wings, but it turns out not to be very significant for temperatures around 25 000 K typical of the white dwarf atmospheres. We conclude that the shift is neither a consequence of the perturber velocity distribution nor of the initial distribution of perturbers due to their interaction with the radiating atom.

Another reason may be the use of the expansion in density to compute the opacities. We have noted the large atom-ion distances at which the Lyman γ satellites are formed. Figure 5 shows that the amplitude of the Lyman γ satellites changes significantly when the proton density is larger than 10^{17} cm^{-3}. For the white dwarfs we have considered here (models with T_{eff} about 21 000 K, and $\log g = 8$), the electron density at the depth of formation of the Lyman β and Lyman γ wings is less than 10^{17} cm^{-3}. Thus it is acceptable to use the density expansion of the correlation function. This would not be the case for massive white dwarfs with higher effective temperature and gravity and this simplifying approximation would no longer be useful because higher electron densities are involved in the atmosphere model calculations [34]. Nevertheless, the use of an expansion in densities in the comparisons shown here would not be a cause of the discrepant shifts.

We have seen in Figure 3 that the shape of the profile in the region of the satellites is very sensitive to the relative strength of these two features. It is therefore very important to have an accurate quantitative determination of the satellite amplitudes. Accurate theoretical molecular potentials have to be used to describe the interaction between the radiator and the perturber in the

work described here. Another important factor, not yet included for Lyman γ, is the variation of the dipole moment during the collision. We have previously shown that the strengths of line satellites are very dependent on values of the electric-dipole moments at the internuclear separation responsible for the satellites [12–14]. Large enhancements in the amplitudes of the satellites may occur whenever the dipole moment increases through the region of internuclear distance where the satellites are formed. The theoretical shape in this region of the profile is then very dependent on the dipole moment of the transition. Our approximation here to consider it as constant may be responsible for some of the differences remaining between the observed and synthetic spectra. This will be improved in future calculations by incorporating R-dependent radiative transition moments for H_2^+.

This paper is dedicated to Henri van Regemorter who died in 2002. His support and interest in the development of the fundamental physics of line broadening is gratefully acknowledged.

References

1. N. Allard, J. Kielkopf, Rev. Mod. Phys. **54**, 1103 (1982)
2. D. Koester, N. Allard, *White Dwarfs: Advances in Observation and Theory* (Kluwer, Dordrecht, 1998), p. 237
3. D. Koester, D. Finley, J.W. Allard, N.F. Kruk, R.A. Kimble, Astrophys. J. **463**, L93 (1996)
4. J. Kielkopf, N. Allard, Phys. Rev. A **58**, 4416 (1998)
5. D. Koester, N.F. Allard, G. Vauclair, Astron. Astrophys. **291**, L9 (1994)
6. H. Holweger, D. Koester, N.F. Allard, Astron. Astrophys. **290**, L21 (1994)
7. P. Bergeron, F. Wesemael, R. Lamontagne, G. Fontaine, R.A. Saffer, N.F. Allard, Astrophys. J. **449**, 358 (1995)
8. D. Koester, U. Sperhake, N.F. Allard, D.S. Finley, S. Jordan, Astron. Astrophys. **336**, 276 (1998)
9. B. Wolff et al., Astron. Astrophys. **373**, 674 (2001)
10. G. Hébrard et al., Astron. Astrophys. **394**, 647 (2002)
11. N. Allard, D. Koester, N. Feautrier, A. Spielfiedel, Astron. Astrophys. Suppl. Ser. **108**, 417 (1994)
12. N. Allard, J. Kielkopf, N. Feautrier, Astron. Astrophys. **330**, 782 (1998)
13. N. Allard, I. Drira, M. Gerbaldi, J. Kielkopf, A. Spielfiedel, Astron. Astrophys. **335**, 1124 (1998)
14. N. Allard, A. Royer, J. Kielkopf, N. Feautrier, Phys. Rev. A **60**, 1021 (1999)
15. M.M. Madsen, J. Peek, At. Data **2**, 171 (1971)
16. J. Power, Phil. Trans. Roy. Soc. A **274**, 663 (1973)
17. J. Power, NRCC Pub. **13199** (1973), not widely distributed, but available on request from the authors
18. D. Bates, R. Reid, Adv. At. Mol. Phys. **4**, 13 (1968)
19. J. Power, Quant. Chem. Prog. Exch. **11**, 233 (1973)
20. D. Ramaker, J. Peek, J. Phys. B: At. Mol. Opt. Phys. **5**, 2175 (1972)
21. D. Ramaker, J. Peek, At. Data **5**, 167 (1973)
22. J. Peek, M. Madsen, Phys. Rev. A **43**, 147 (1991)
23. P. Anderson, J. Talman, Bell Sys. Tech. Pub. **3117**, 29 (1956)
24. J. Kielkopf, N. Allard, Phys. Rev. Lett. **43**, 196 (1979)
25. N. Allard, J. Phys. B.: At. Mol. Opt. Phys. **11**, 1383 (1978)
26. A. Royer, Acta Phys. Pol. A **54**, 805 (1978)
27. A. Royer, Phys. Rev. A **43**, 499 (1971)
28. J. Kielkopf, N. Allard, Astrophys. J. **450**, L75 (1995)
29. A. Spielfiedel, J. Mol. Spec. **217**, 162 (2002)
30. I. Hubeny, Comp. Phys. Comm. **52**, 103 (1988)
31. I. Hubeny, T. Lanz, Astron. Astrophys. **262**, 501 (1992)
32. I. Hubeny, T. Lanz, Astrophys. J. **439**, 875 (1995)
33. G. Hébrard et al., Astron. Astrophys. **405**, 1153 (2003)
34. J. Dupuis, P. Chayer, S. Vennes, G. Hebrard, N.F. Allard, Astrophys. J. **598**, 486 (2003)